J. Fluid Mech. (2024), *vol*. 996, A42, doi:10.1017/jfm.2024.585

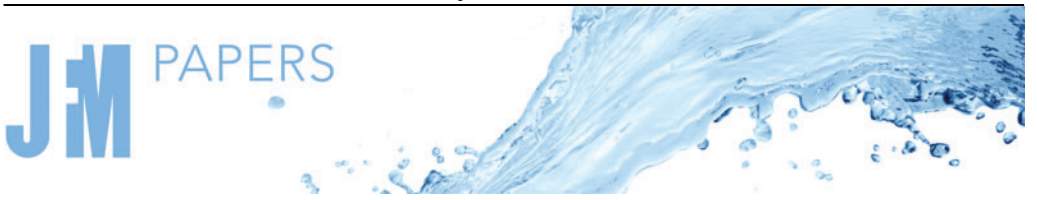

The spatial Whitham equation

John D. Carter[1],†, **Diane Henderson**[2] **and Panayotis Panayotaros**[3]

[1]Mathematics Department, Seattle University, 901 12th Ave, Seattle, WA 98122, USA

[2]Department of Mathematics, Penn State University, 218 McAllister Building, University Park, PA 16802, USA

[3]Instituto de Investigaciones en Matemáticas Aplicadas y en Sistemas, Universidad Nacional Autónoma de México, Apdo. Postal 20-716, 01000 Cd. México, México

(Received 22 February 2024; revised 14 June 2024; accepted 7 July 2024)

The Whitham equation is a non-local, nonlinear partial differential equation that models the temporal evolution of spatial profiles of surface displacement of water waves. However, many laboratory and field measurements record time series at fixed spatial locations. To directly model data of this type, it is desirable to have equations that model the spatial evolution of time series. The spatial Whitham (sWhitham) equation, proposed as the spatial generalization of the Whitham equation, fills this need. In this paper, we study this equation and apply it to water-wave experiments on shallow and deep water. We compute periodic travelling-wave solutions to the sWhitham equation and examine their properties, including their stability. Results for small-amplitude solutions align with known results for the Whitham equation. This suggests that the systems are consistent in the weakly nonlinear regime. At larger amplitudes, there are some discrepancies. Notably, the sWhitham equation does not appear to admit cusped solutions of maximal wave height. In the second part, we compare predictions from the temporal and spatial Korteweg–de Vries and Whitham equations with measurements from laboratory experiments. We show that the sWhitham equation accurately models measurements of tsunami-like waves of depression, waves of elevation, and solitary waves on shallow water. Its predictions also compare favourably with experimental measurements of waves of depression and elevation on deep water. Accuracy is increased by adding a phenomenological damping term. Finally, we show that neither the sWhitham nor the temporal Whitham equation accurately models the evolution of wave packets on deep water.

Key words: surface gravity waves, general fluid mechanics

† Email address for correspondence: carterj1@seattleu.edu

1. Introduction

We investigate the spatial Whitham (sWhitham) equation, proposed by Trillo *et al.* (2016), for gravity waves propagating on the surface of water. This equation was motivated by the success of the temporal Korteweg–de Vries (tKdV) and temporal Whitham (tWhitham) equations in modelling the evolution of unidirectional waves in shallow water. The tWhitham equation uses a more accurate linear dispersive term than the tKdV equation and therefore may be useful for depths ranging from shallow to deep. The tWhitham equation can also approximate some singularity formation effects, see Whitham (1967) and Ehrnström & Wahlén (2019). Comparisons with experimental data suggest the tWhitham equation improves on the tKdV equation in the small-amplitude long-wave regime, see Trillo *et al.* (2016) and Carter (2018).

A limitation of temporal models is that they describe how a given surface displacement profile evolves in time. However, many field and laboratory experiments provide temporal profiles of the surface displacement at fixed spatial locations and ask how these temporal profiles evolve in space. This problem arises in many wave phenomena, e.g. in optics, and there is a long use of 'spatial evolution' equations that describe how a signal, e.g. an optical image, changes along some direction in space. Despite their motivation, spatial equations have not been used systematically for nonlinear dispersive water-wave models. Herein, we examine a recently proposed model, the sWhitham equation of Trillo *et al.* (2016), and show evidence that this equation can improve on predictions of the tWhitham, tKdV and spatial KdV (sKdV) equations. We consider this equation mathematically, numerically and experimentally and compare its properties and predictions with those of the tKdV, tWhitham and sKdV equations. Our results yield new information on the properties of the sWhitham equation and its strengths and limitations as a model of unidirectional water waves.

The motion of a two-dimensional, irrotational, incompressible, inviscid fluid on a horizontal, impermeable bed can be modelled by

$$\phi_{xx} + \phi_{zz} = 0, \quad \text{for } -h_0 < z < \eta, \tag{1.1a}$$

$$\phi_t + \tfrac{1}{2}|\nabla\phi|^2 + g\eta = 0, \quad \text{at } z = \eta, \tag{1.1b}$$

$$\eta_t + \eta_x\phi_x = \phi_z, \quad \text{at } z = \eta, \tag{1.1c}$$

$$\phi_z = 0, \quad \text{at } z = -h_0, \tag{1.1d}$$

where $\phi(x, z, t)$ represents the velocity potential of the fluid, $\eta(x, t)$ represents the surface displacement of the fluid, g represents the acceleration due to gravity, h_0 represents the uniform depth of the fluid at rest and x, z, t represent the horizontal, vertical and temporal coordinates, respectively. See Johnson (2001) for details of this system. Since this system is a nonlinear free-boundary problem, approximate models are often used. Linear theory gives the dispersion relation

$$\omega^2 = g\kappa \tanh(\kappa h_0), \tag{1.2}$$

where κ and ω are the wavenumber and angular frequency of the linear wave, respectively.

The dimensional tKdV equation (Korteweg & de Vries 1895),

$$\eta_t + \sqrt{gh_0}\,\eta_x + \frac{1}{6}h^2\sqrt{gh_0}\,\eta_{xxx} + \frac{3}{2h_0}\sqrt{gh_0}\,\eta\eta_x = 0, \tag{1.3}$$

is a small-amplitude, long-wave approximation of (1.1). The tKdV equation has been well studied mathematically (e.g. Ablowitz & Segur 1981; Miles 1981; Lannes 2013) and

experimentally (e.g. Russell 1844; Zabusky & Galvin 1971; Hammack 1973; Hammack & Segur 1978). It has dispersion relation

$$\omega_{\mathrm{KdV}} = \sqrt{gh_0}\left(\kappa - \tfrac{1}{6}h_0^2\kappa^3\right). \tag{1.4}$$

Equation (1.4) is a unidirectional approximation of (1.2) that is valid in the long-wave (i.e. $\kappa h_0 \to 0$) limit. In order to obtain a weakly nonlinear approximation to (1.1) that is valid for a wider range of κh_0 values, Whitham (1967, 1974) proposed the following dimensional equation:

$$\eta_t + \sqrt{\frac{g}{h_0}}\,\mathcal{K}(\kappa) * \eta + \frac{3}{2h_0}\sqrt{gh_0}\,\eta\eta_x = 0, \tag{1.5}$$

as a model for the evolution of small-amplitude waves on shallow water. We refer to (1.5) as the dimensional tWhitham equation. The convolution term is defined by

$$\mathcal{K}(\kappa) * \eta = \tilde{\mathcal{F}}^{-1}\left(\mathcal{K}(\kappa)\tilde{\mathcal{F}}(\eta)\right), \tag{1.6}$$

where $\mathcal{K}(\kappa)$ is the non-dimensional Fourier multiplier given by

$$\mathcal{K}(\kappa) = i\,\mathrm{sgn}(\kappa)\sqrt{\kappa h_0 \tanh(\kappa h_0)}, \tag{1.7}$$

and $\tilde{\mathcal{F}}$ and $\tilde{\mathcal{F}}^{-1}$ represent the Fourier and inverse Fourier transforms in x, respectively. We write the tWhitham equation and $\mathcal{K}$ in forms different than those used by Whitham in order to simplify the work below. The linear dispersion relation for the tWhitham equation is

$$\omega_W = \mathrm{sgn}(\kappa)\sqrt{g\kappa \tanh(\kappa h_0)}. \tag{1.8}$$

Equation (1.8) is one root of (1.2), which means that the tWhitham equation exactly models the wave speed of unidirectional linear waves for any κh_0.

Given an initial spatial profile of the surface displacement (i.e. given η for all values of x at $t = 0$), (1.3) and (1.5) provide predictions for the spatial profiles of η for $t > 0$. Because of this requirement for initial spatial data, these equations are known as evolution-in-time or 'temporal' equations. Many laboratory and field water-wave measurements are made by recording time series at fixed spatial locations (i.e. using stationary gauges or buoys to collect time series). Evolution-in-space or 'spatial' equations are required to directly compare with measurements of this type. In these situations, time series at the first measurement location are used as initial conditions in spatial equations that are solved to obtain predictions for the time series at the downstream measurement locations. Spatial equations are commonly used in nonlinear optics, e.g. in the study of pulse propagation in optical fibres, see for e.g. Manakov (1974) and Agrawal (2019).

Three common methods used for deriving approximate spatial equations from (1.1) include the following: (i) interchanging the roles of x and t in the derivation of the temporal equations; (ii) starting with an approximate temporal equation and then applying the change of variables $\eta_t \sim -\sqrt{gh_0}\,\eta_x$ for waves in shallow water; (iii) inverting the

dispersion relation. Using either (i) or (ii) gives the dimensional sKdV equation

$$\eta_x + \frac{1}{\sqrt{gh_0}}\,\eta_t - \frac{\sqrt{gh_0}}{6g^2}\,\eta_{ttt} - \frac{3}{2h_0\sqrt{gh_0}}\,\eta\eta_t = 0. \tag{1.9}$$

Using method (i) for the nonlinear part and method (iii) for the linear part, Trillo *et al.* (2016) proposed the following dimensional sWhitham equation:

$$\eta_x + \sqrt{\frac{h_0}{g}}\,\mathcal{K}^{-1}(\omega) * \eta - \frac{3}{2h_0\sqrt{gh_0}}\,\eta\eta_t = 0, \tag{1.10}$$

where the convolution term is defined by

$$\mathcal{K}^{-1}(\omega) * \eta = \mathcal{F}^{-1}\left(\mathcal{K}^{-1}(\omega)\mathcal{F}(\eta)\right), \tag{1.11}$$

using $\mathcal{F}$ and $\mathcal{F}^{-1}$ to represent the Fourier and inverse Fourier transforms in t, respectively, and $\mathcal{K}^{-1}(\omega)$ as the inverse of $\mathcal{K}(\kappa)$. Although a closed-form expression for $\mathcal{K}^{-1}(\omega)$ is not known, the inverse is guaranteed to exist since $\mathcal{K}(\kappa)$ is one-to-one and onto for $\kappa \in \mathbb{R}$. In general, if the dispersion is monotonic and onto, then the linear initial-value problem can be written in spatial form. In other words, one can recover the spatial initial condition from the time series at $x = 0$ and *vice versa*. Note that if weak surface tension were included, then $\mathcal{K}(\kappa)$ would not be one-to-one and a unique inverse would not exist.

In the following, we consider both the mathematical properties of the sWhitham equation and its applications. Section 2 includes a summary of the mathematical properties including its conserved quantities, travelling-wave solutions and their stability. Section 3 contains comparisons between measurements from laboratory experiments and predictions obtained from the tKdV, sKdV, tWhitham and sWhitham equations, and their dissipative generalizations. Section 4 contains a summary of the results.

2. Properties of the spatial equations

In order to gain an understanding of the sWhitham equation, we present its properties along with the properties of the sKdV equation for comparative purposes. We define non-dimensional variables u, χ and τ by

$$u = \frac{\eta}{h_0}, \quad \chi = \frac{x}{h_0}, \quad \tau = \sqrt{\frac{g}{h_0}}\,t. \tag{2.1a–c}$$

The corresponding non-dimensional sKdV equation is

$$u_\chi + u_\tau - \tfrac{1}{6}u_{\tau\tau\tau} - \tfrac{3}{2}uu_\tau = 0, \tag{2.2}$$

and the non-dimensional sWhitham equation is

$$u_\chi + K^{-1}(w) * u - \tfrac{3}{2}uu_\tau = 0, \tag{2.3}$$

where $w = \sqrt{h_0/g}\,\omega$ is the non-dimensional circular frequency and K is the non-dimensional Fourier multiplier defined by

$$K(k) = i\,\mathrm{sgn}(k)\sqrt{k\tanh(k)}, \tag{2.4}$$

where $k = h_0\kappa$ is the non-dimensional wavenumber.

2.1. *Conserved quantities*

The sKdV equation is known to have an infinite number of conservation laws, see for example Ablowitz & Segur (1981). The first three conserved quantities are

$$\tilde{\mathcal{Q}}_1 = \int_{-\infty}^{\infty} u \,\mathrm{d}\tau, \tag{2.5a}$$

$$\tilde{\mathcal{Q}}_2 = \int_{-\infty}^{\infty} u^2 \,\mathrm{d}\tau, \tag{2.5b}$$

$$\tilde{\mathcal{Q}}_3 = \tfrac{1}{2}\int_{-\infty}^{\infty} \left(u^2 + \tfrac{1}{6}u_\tau^2 - \tfrac{1}{2}u^3\right) \mathrm{d}\tau, \tag{2.5c}$$

where $\mathcal{Q}_3$ is the Hamiltonian. The sWhitham equation conserves $\tilde{\mathcal{Q}}_1$,$\tilde{\mathcal{Q}}_2$ and its Hamiltonian

$$\tilde{\mathcal{Q}}_4 = \frac{1}{2}\int_{-\infty}^{\infty} \left(u\left(\frac{K^{-1}(w)}{iw}\right) * u - \frac{1}{2}u^3\right) \mathrm{d}\tau. \tag{2.6}$$

The quantities $\mathcal{Q}_1$ and $\mathcal{Q}_2$ are sometimes referred to as the mass and momentum integrals, respectively. These interpretations are discussed in depth in Ali & Kalisch (2014). We emphasize that the quantities $\tilde{\mathcal{Q}}_1$ to $\tilde{\mathcal{Q}}_4$ are constant in χ, the non-dimensional spatial variable. The periodic generalizations of these conserved quantities, $\tilde{\mathcal{Q}}_1$, $\tilde{\mathcal{Q}}_2$, $\tilde{\mathcal{Q}}_3$, $\tilde{\mathcal{Q}}_4$, for the tKdV, sKdV, tWhitham and sWhitham equations are included in the Appendix A.

2.2. *Travelling-wave solutions*

The sKdV equation admits a two-parameter family of travelling-wave solutions given by

$$u(\chi,\tau) = U_0 + U_2 \,\mathrm{cn}^2\left(\frac{2E_1(m)}{T}\left(\tau - \gamma\chi\right), m\right), \tag{2.7}$$

where

$$U_0 = -\frac{16}{3T^2}E_1(m)\left(E_2(m) + (m-1)E_1(m)\right), \tag{2.8a}$$

$$U_2 = \frac{16m}{3T^2}\left(E_1(m)\right)^2, \tag{2.8b}$$

$$\gamma = 1 + \frac{8}{3T^2}(m-2)\left(E_1(m)\right)^2 + \frac{8}{T^2}E_1(m)E_2(m). \tag{2.8c}$$

Here T is the (temporal) period of the solution, U_2 is the wave height of the solution, $m \in [0,1)$ is known as the elliptic parameter of the Jacobi elliptic function $\mathrm{cn}(\cdot, m)$, and $E_1(m)$ and $E_2(m)$ are the complete elliptic integrals of the first and second kinds, respectively. See Byrd & Friedman (1971) for details of elliptic functions. Without loss of generality, the integration constant, U_0, was chosen so that the solutions have zero mean (i.e. $\mathcal{Q}_1 = 0$) because (2.7) is invariant under the transformation

$$U_0 \to U_0 + \nu, \quad \gamma \to \gamma - \tfrac{3}{2}\nu, \tag{2.9a,b}$$

where ν is any real constant. The two-parameter family (the free parameters are T and m) of solutions given in (2.7) comprises all zero-mean, travelling-wave solutions to the sKdV equation. A profile of the form $u(\tau - \gamma\chi)$ of the spatial equation is interpreted as

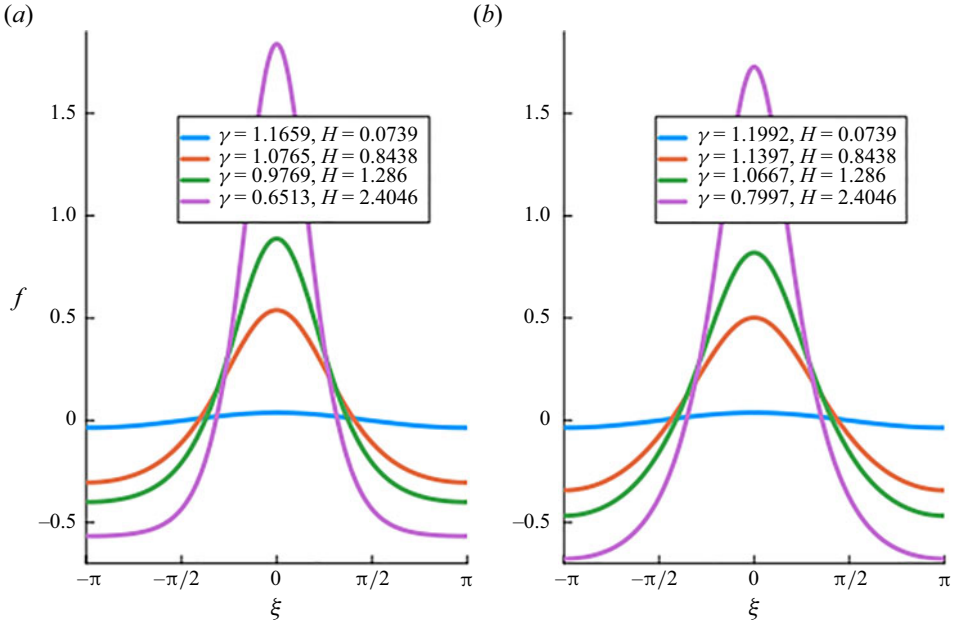

Figure 1. Plots of four 2π-periodic, zero-mean, travelling-wave solutions to (*a*) the sKdV equation and (*b*) the sWhitham equation. The γ values and wave heights, H, are included in the legends.

the $u(-\gamma(x-\gamma^{-1}t))$ travelling-wave profile of the temporal evolution. This means that the non-dimensional real parameter γ corresponds to the inverse of the non-dimensional wave speed.

Figure 1(*a*) contains plots of four 2π-periodic solutions of the sKdV equation. The wave heights, H, and γ values for these solutions are included in the legend. The sKdV equation does not admit a solution with maximal height, nor does it admit a solution with minimal γ value. As $m \to 1$, H increases without bound, and γ decreases without bound. Once the height of the solution becomes large enough, the γ value becomes negative. For solutions with period $T = 2\pi$, this sign transition occurs for solutions with height $H \approx 4.28$. Since γ is the inverse of wave speed, γ going through zero corresponds to the wave speed going to infinity. This non-physical result may be due to the fact that the sWhitham equation is a generalization of the sKdV equation, which is a model of small-amplitude waves, and these waves are well outside the small-amplitude regime.

Ehrnström & Kalisch (2009) proved that the tWhitham equation admits small-amplitude, periodic travelling-wave solutions and computed some of these solutions. Ehrnström & Wahlén (2019) proved Whitham's conjecture that the tWhitham equation admits a travelling-wave solution with maximal wave height and that this solution is cusped. Carter (2024) numerically examined the properties of solutions to the tWhitham equation close to the maximal height.

We consider periodic travelling-wave solutions of the sWhitham equation of the form

$$u(\chi,\tau) = f(\tau - \gamma\chi) = f(\xi), \tag{2.10}$$

where γ is a real constant and f is a smooth, real-valued function of $\xi = \tau - \gamma\chi$ with non-dimensional temporal period T. Substituting (2.10) into (2.3) and integrating with

respect to ξ once gives

$$-\gamma f + \left(\frac{K^{-1}(w)}{i\,w}\right) * f - \frac{3}{4}f^2 = B, \tag{2.11}$$

where B is the constant of integration. This equation is invariant under the transformation

$$f \to f + \nu, \quad \gamma \to \gamma - \tfrac{3}{2}\nu, \quad B \to B + \nu\left(\gamma - \tfrac{3}{4}\nu\right), \tag{2.12a–c}$$

where ν is any real constant. Therefore, without loss of generality, we only consider travelling-wave solutions of the sWhitham equation that have zero mean.

Equation (2.11) can be solved approximately by assuming f has a Fourier expansion of the form

$$f(\xi) = \sum_{j=-N}^{N} \hat{f}(j) \exp\left(\frac{2\pi \mathrm{i} j \xi}{T}\right), \tag{2.13}$$

where N is a large positive integer and the $\hat{f}$ are complex constants. Since f has zero mean, $\hat{f}(0) = 0$. For simplicity, we assume that the solutions are real and even. Thus, $\hat{f}(-j) = \hat{f}(j)$ for $j = 1, \ldots, N$. Substituting (2.13) into (2.11) gives

$$-\gamma\hat{f}(j) + \frac{TK^{-1}\left(\dfrac{2\pi w}{T}\right)}{2\pi i w}\hat{f}(j) - \frac{3}{4}\sum_{l=-N+j}^{N} \hat{f}(j-l)\hat{f}(l) = 0, \quad \text{for } j = 1, 2, \ldots, N. \tag{2.14}$$

We solved this system of nonlinear algebraic equations for the $\hat{f}$ using Newton's method (see Ehrnström & Kalisch (2009) and Carter *et al.* (2022) for the details in closely related problems).

Figure 1(*b*) includes plots of four 2π-periodic, zero-mean, travelling-wave solutions to the sWhitham equation. As the value of γ decreases, the height of the solution increases. For the sWhitham equation, the γ value for 2π-periodic solutions becomes negative when $H \approx 3.70$. We do not see evidence of a wave of maximum height that is analogous to the cusped wave seen in the tWhitham equation, see Ehrnström & Wahlén (2019). This result is consistent with the fact that stronger dispersion typically has a regularizing effect.

Figure 2 includes plots of four travelling-wave solutions to the sWhitham equation with period $T = 10\pi$. Just as in the $T = 2\pi$ case, there does not appear to be a solution with maximal height, nor a solution with minimal γ value. However, once the height becomes large enough, the solutions no longer increase monotonically on $\xi \in (-5\pi, 0)$. This is demonstrated in the inset plot in figure 2. This non-monotonic behaviour is not a numerical artefact. We checked that the purple solution is in fact a travelling-wave solution by evolving it for multiple periods in evolution code for the sWhitham equation. This non-monotonic behaviour is not exhibited by solutions to the sKdV, tKdV or tWhitham equations. Finally, the sWhitham equation does not meet the criteria for monotonic growth presented in Bruell & Pei (2023). For clarity, we define height by $H = \max(u) - \min(u)$ regardless if the solution is monotonic on $\xi \in (-T/2, 0)$ or not.

2.3. *Stability of travelling-wave solutions*

Benjamin & Feir (1967) showed that small-amplitude periodic travelling-wave solutions to (1.1) are stable with respect to the modulational instability (long-wavelength perturbations)

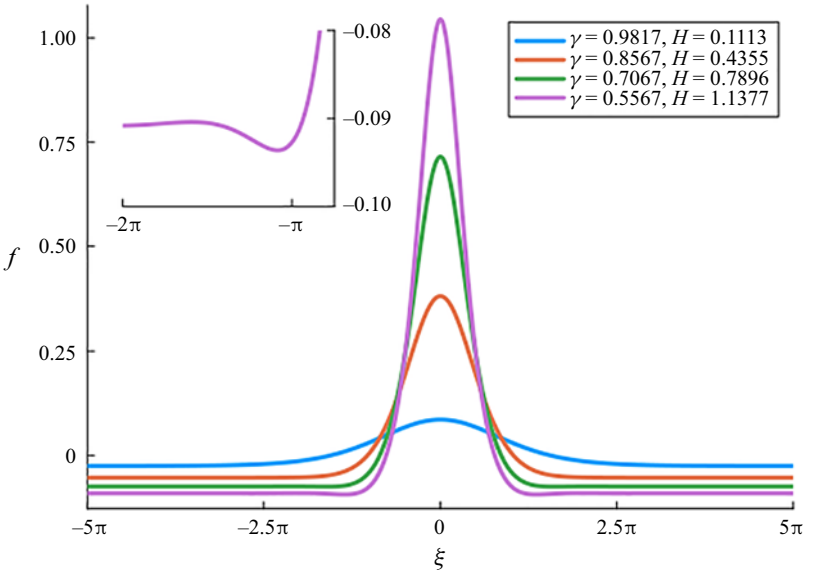

Figure 2. Plots of four travelling-wave solutions to the sWhitham equation with period $T = 10\pi$. The inset plot shows that the solutions are not monotonic on $\xi \in (-5\pi, 0)$ when the solution height is sufficiently large.

when $2\pi/L < 1.363$ and are unstable with respect to the modulational instability when $2\pi/L > 1.363$, where L is the spatial wavelength. Bottman & Deconinck (2009) and Deconinck & Nivala (2010) proved that all travelling-wave solutions of the tKdV equation are stable regardless of their height or (spatial) period. Due to the similarities between the tKdV and sKdV equations, these results also establish that all travelling-wave solutions of sKdV are stable regardless of their height or period. Hur & Johnson (2015) proved that travelling-wave solutions to the tWhitham equation with sufficiently small amplitude are stable with respect to the modulational instability if $2\pi/L < 1.146$ and are unstable with respect to the modulational instability otherwise. The more general work of Binswanger *et al.* (2021) also shows that the small-amplitude modulational instability cutoff occurs at $2\pi/L = 1.146$ in the tWhitham equation. Sanford *et al.* (2014) numerically corroborated these results. They numerically showed that all periodic travelling-wave solutions of the tWhitham equation with large enough amplitude, regardless of wavelength, are unstable. Additionally, they showed that these large-amplitude solutions are unstable with respect to perturbations of all wavelengths greater than or equal to that of the unperturbed solution. Finally, they showed that the instability growth rate increases monotonically with the solution height.

Applying equation (23) of Binswanger *et al.* (2021) to the sWhitham equation establishes that all small-amplitude periodic travelling-wave solutions are stable with respect to the modulational instability regardless of their period. This result is qualitatively similar to the tKdV and sKdV results, but is qualitatively different than the tWhitham result.

In order to numerically study the stability of travelling-wave solutions to the sWhitham equation, we employ the Fourier–Floquet–Hill method of Deconinck & Kutz (2006). First, enter a coordinate frame moving with the solution via the change of variables

$$\xi = \tau - \gamma\chi. \tag{2.15}$$

This converts (2.3) to

$$u_\chi - \gamma u_\xi + K^{-1}(w) * u - \tfrac{3}{2} u u_\xi = 0, \tag{2.16}$$

and converts travelling-wave solutions of (2.3) into stationary (i.e. $\partial_\chi u = 0$) solutions of (2.16). Next, consider perturbed solutions of the form

$$u_{pert}(\xi, \chi) = u(\xi) + \epsilon v(\xi, \chi) + O(\epsilon^2), \tag{2.17}$$

where u is a periodic travelling-wave solution of the sWhitham equation, ϵ is a small real constant and ϵv is the leading-order part of the perturbation. Substituting (2.17) into (2.16) and linearizing gives

$$v_\chi - \gamma v_\xi + K^{-1}(w) * v - \tfrac{3}{2} u' v - \tfrac{3}{2} u v_\xi = 0, \tag{2.18}$$

where 'prime' means derivative with respect to ξ. Without loss of generality assume

$$v(\xi, \chi) = V(\xi) \mathrm{e}^{\lambda \chi} + \text{c.c.}, \tag{2.19}$$

where V is a complex-valued function, λ is a complex constant whose real part corresponds to the growth rate of the instability and c.c. stands for complex conjugate. Substituting (2.19) into (2.18) and rearranging gives

$$\gamma V' - K^{-1}(w) * V + \tfrac{3}{2} u' V + \tfrac{3}{2} u V' = \lambda V. \tag{2.20}$$

All bounded solutions to this equation (i.e. solutions with any period) have the form $V(\xi) = \mathrm{e}^{\mathrm{i}\mu\xi} W(\xi)$, where W is a T-periodic function and $\mu \in [-\pi/T, \pi/T]$ is a constant known as the Floquet parameter, see Deconinck & Kutz (2006). This gives

$$V(\xi) = \mathrm{e}^{\mathrm{i}\mu\xi} \sum_{j=-\infty}^{\infty} \hat{W}(j) \mathrm{e}^{2\pi \mathrm{i} j \xi / T}, \tag{2.21}$$

where the $\hat{W}(j)$ are complex numbers. In our numerical computations, we use the truncation

$$V(\xi) = \mathrm{e}^{\mathrm{i}\mu\xi} \sum_{j=-N}^{N} \hat{W}(j) \mathrm{e}^{2\pi \mathrm{i} j \xi / T}, \tag{2.22}$$

where N is a large positive integer. If there exists a bounded solution to (2.20) with λ that has a positive real part, then the perturbation grows exponentially in χ and the corresponding solution to the sWhitham equation is said to be unstable. If all solutions of (2.20) have λ values that are purely imaginary, then the corresponding solution is said to be spectrally stable.

Travelling-wave solutions to the sWhitham equation with period $T = 2\pi$, height $H < 0.842$ and $\gamma > 1.14$ are spectrally stable. As the wave height surpasses $H = 0.842$ (and γ falls below 1.14), the solutions become unstable. The spectra corresponding to solutions with heights just above the critical value are oval-like shapes centred at the origin. The oval-like shapes correspond to perturbations with μ values near ± 0.5. (A perturbation with $\mu = 0.5$ has a period that is twice that of the unperturbed solution.) As the height increases further, more μ values lead to instability and the ovals transition into lemniscates centred at the origin. All non-zero μ values lead to instability when the complete lemniscate is formed. For solutions with period 2π, the complete lemniscate is

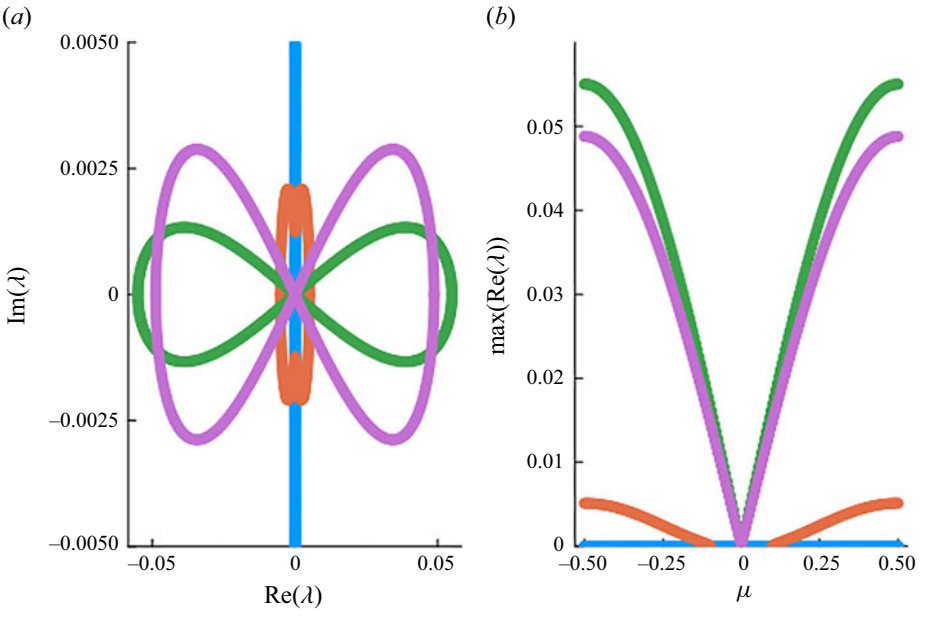

Figure 3. Plots of the stability results for the sWhitham solutions with $T = 2\pi$ shown in figure 1(*b*). The coloured curves in this figure correspond to the solutions of the same colours in figure 1(*b*). Panel (*a*) shows the stability spectra and (*b*) shows the maximum growth rate versus the Floquet parameter.

first observed near $H = 0.845$. These sWhitham stability results are qualitatively different than the tWhitham results where the first unstable solutions have spectra with lemniscates centred at the origin. Such spectra are created by perturbations with μ values near zero and are representative of the modulational instability.

Figure 3(*a*) includes plots of the stability spectra for the sWhitham solutions shown in figure 1(*b*). Figure 3(*b*) includes plots of $\max(\mathrm{Re}(\lambda))$, i.e. the maximal instability growth rate, versus μ for the same solutions. The solution with smallest height (coloured blue in the plots) is spectrally stable since it has a purely imaginary spectrum. The fact that this solution is stable is consistent with the Binswanger *et al.* (2021) asymptotic result that all travelling-wave solutions of the sWhitham equation with sufficiently small amplitudes are stable with respect to the modulational instability. Additionally, this solution does not exhibit the 'bubble' instabilities seen in the Euler equations, see Deconinck & Oliveras (2011), or in bidirectional generalizations of the tWhitham equation, see Deconinck & Trichtchenko (2015). The other three solutions plotted in figure 1 are unstable.

The solution with second smallest height (coloured orange) is unstable. Its stability spectrum is an oval-like shape centred at the origin that is transitioning into a lemniscate, see figure 3(*a*). This sWhitham solution is only unstable with respect to perturbations with approximately $|\mu| \in [0.1, 0.5]$. Since μ near zero does not lead to instability, this solution is stable with respect to the modulational instability. The solution is most unstable with respect to perturbations with $\mu = 0.5$. This means that perturbations with period $T = 4\pi$, i.e. twice the period of the underlying solution, grow fastest. These results are qualitatively different than those obtained for moderate-amplitude 2π-periodic travelling-wave solutions of the tWhitham equation, see Sanford *et al.* (2014).

The solution with the third smallest height (coloured green in the plots) is unstable with respect to perturbations with any non-zero value of μ. The stability spectrum is a

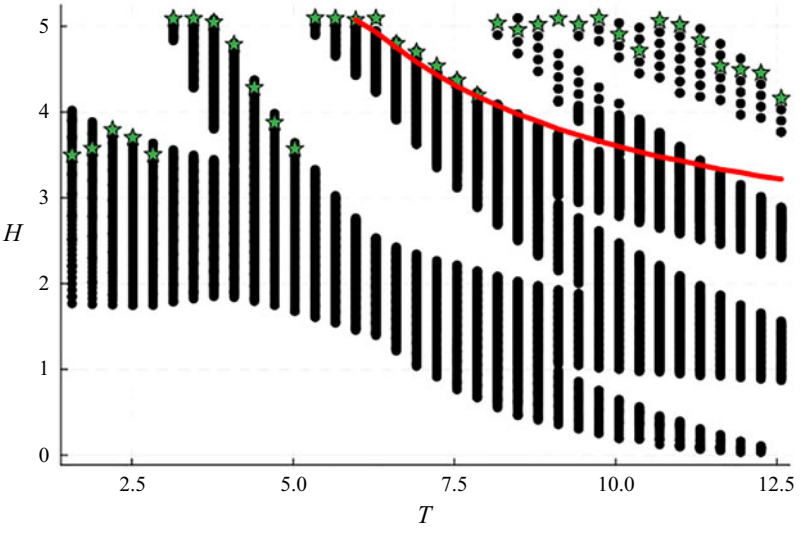

Figure 4. Plot of the regions of (T, H)-space for which periodic travelling-wave solutions of the sWhitham equation are unstable (black dots) with respect to the $\mu = 0.5$ instability. Solutions corresponding to (T, H) in the white bands are stable with respect to $\mu = 0.5$ perturbations. The green stars represent the approximate location of the most unstable solutions for that period. The red curve shows the approximate values of (T, H) where γ becomes negative.

lemniscate centred at the origin. The instability growth rates for this solution are larger than those for the solution with the second smallest height. It is most unstable with respect to the perturbation with $\mu = 0.5$, a perturbation with $T = 4\pi$. Finally, the solution with the largest height (coloured magenta) is also unstable with respect to perturbations with any non-zero μ and its stability spectrum is a lemniscate centred at the origin. However, the growth rates of the instabilities of this solution are smaller than the growth rates of the solution with third smallest wave height, see figure 3(*b*).

As the wave height continues to increase, there are alternating bands of stability and instability. Figure 4 shows regions of (T, H)-space for which periodic travelling-wave solutions to the sWhitham equation are unstable with respect to $\mu = 0.5$ perturbations (black dots). For this plot, we only examined $\mu = 0.5$ perturbations because for all (T, H) pairs we examined, the $\mu = 0.5$ perturbation had the largest instability growth rate. There does not appear to be a simple relationship between (T, H) and stability. For example, all four of the 10π-periodic solutions shown in figure 2 are stable, but not all 10π-periodic solutions are stable. The approximate values of (T, H) where γ turns negative are shown by the red curve. This curve does not appear to have a simple relationship with stability. Figure 4 shows that there are bands of instability and stability. This is qualitatively different than what happens in the tWhitham case where all large-amplitude solutions are unstable and the growth rate increases monotonically with wave height. It is unintuitive that some large-amplitude solutions are stable. This unintuitive result may be attributed to the fact that the sWhitham equation is a model for small-amplitude waves and these solutions are outside of that range of validity.

Finally, we did not find any solutions to the sWhitham equation that are unstable with respect to the superharmonic instability, a perturbation that has the same period as the solution (i.e. $\mu = 0$). Additionally, neither $\mathcal{Q}_2$ nor $\mathcal{Q}_3$ oscillate for the sWhitham equation as solution height increases. These results are qualitatively different than the

tWhitham case where travelling-wave solutions with large-enough amplitude are unstable with respect to the superharmonic instability, see Carter *et al.* (2023).

3. Comparisons with experiments

The tKdV equation has been shown to compare favourably with experiments, see for example Russell (1844), Zabusky & Galvin (1971), Hammack (1973), Hammack & Segur (1974) and Hammack & Segur (1978). Trillo *et al.* (2016) showed that both the sKdV and sWhitham equations accurately model the evolution of experimental waves of depression on shallow water. Carter (2018) showed that the tWhitham equation more accurately predicts the evolution of experimental waves of depression than do the tKdV and Serre equations.

In this section, we present comparisons between predictions obtained from numerical simulations of the model equations and measurements from four different series of laboratory experiments including waves of depression and elevation on shallow water (§§ 3.2 and 3.3), solitons on shallow water (§ 3.4), waves of depression and elevation on deep water (§ 3.5) and wave packets on deep water (§ 3.6).

3.1. *Numerical methods*

In order to make comparisons with measurements from laboratory experiments, the model equations need to be solved numerically. The tKdV and tWhitham equations are solved numerically using fourth-order operator-splitting in time (see Yoshida 1990) and periodic boundary conditions in space. The nonlinear parts of the equations are solved using fourth-order Runge–Kutta in time and a Fourier pseudospectral evaluation of the nonlinearity on a uniform grid (pointwise multiplication in space and spectral computation of the derivative). The linear part of the equations is solved exactly in Fourier space. We use the fast Fourier transform to move between the spatial and spectral variables. The length of the numerical tank must be large enough that waves do not leave one end of the domain, wrap around and impact waves on the other end of the domain. Additionally, the spatial gridpoints must be selected to line up with the experimental gauge locations. As a check on the results, the numerical preservation of the conserved quantities of the equations, see the Appendix A, was monitored.

The sKdV and sWhitham equations are solved using the same methods except that space and time are interchanged. The inverse $K^{-1}(w)$ is evaluated numerically using Newton's method. As a check on the results, the preservation of the conserved quantities, see the Appendix A, was monitored.

3.2. *Waves of depression and elevation on shallow water*

Hammack & Segur (1978) conducted a series of water-wave experiments in a long, narrow tank with $h_0 = 10$ cm, and a wavemaker at one end. The wavemaker was a rectangular, vertically moving piston located on the bottom of the tank next to a rigid wall at one end of the tank. The piston spanned the width of the tank and had a length of 61 cm, so the initial wavelength was 122 cm. This experiment is in the shallow-water regime because the ratio $r = h_0/L = 0.082 \ll 1$ and $\tanh(2\pi r) = 0.47$. The experiments were initialized by rapidly moving the piston downward a prescribed amount. Time series were collected by wave gauges located $61 + 500j$ cm for $j = 0, \ldots, 4$ from the upstream end of the tank. This means that the first gauge was located at the downstream edge of the wavemaker. The tank was long enough that waves reflecting from the downstream end of the tank did not impact the time series.

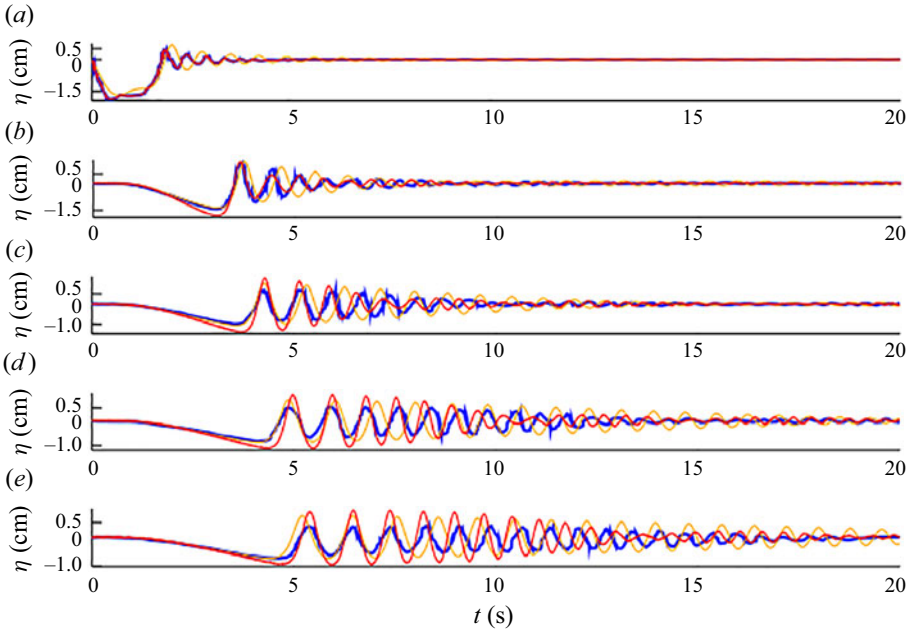

Figure 5. The experimental time series (blue curve) from the Hammack & Segur (1978) experiment using $A_0 = 1.5$ cm with the predictions obtained from the tKdV (orange curve) and sKdV (red curve) equations. The plots are ordered from (*a*) to (*e*) by increasing distance from the wavemaker.

We compare predictions from the tKdV, sKdV, tWhitham and sWhitham equations. The time series collected by the first gauge were used as initial conditions for the simulations of the spatial equations. The initial conditions for the temporal equations require knowledge of the surface displacement for all values of x at the initial time, but that information was not recorded in these experiments. To approximate it, we used the following function as initial condition for the temporal equations:

$$\eta(x,0) = \begin{cases} 0 & -7869 \leqslant x < -183, \\ -\frac{1}{2}A_0 + \frac{1}{2}A_0\,\mathrm{sn}(0.0925434x,\, 0.9999^2) & -183 \leqslant x \leqslant 61, \\ 0 & 61 < x \leqslant 7747, \end{cases} \tag{3.1}$$

where A_0 is the amplitude of the piston motion in centimetres, x is measured in centimetres and $\mathrm{sn}(\cdot, m)$ is a Jacobi elliptic function with elliptic modulus m, see Byrd & Friedman (1971). This function represents a trough of 122 cm centred at $x = -61$ cm.

Figure 5 contains plots comparing the experimental time series with the predictions obtained from the tKdV and sKdV equations for the experiment with $A_0 = 1.5$ cm. Both equations do a reasonable job of predicting the experimental measurements. However, the sKdV equation more accurately predicts the phase speed. (This is especially visible at the downstream gauges.) It is important to note that part of the error in the tKdV prediction is due to the fact that the initial surface is estimated. This is a shortcoming of the temporal equations. Both models overpredict the amplitudes at the downstream gauges and this overprediction increases as the waves travel down the tank. This overprediction is due to the fact that both tKdV and sKdV are conservative models and the experiment contains dissipation. See § 3.3 for a discussion of the role dissipation plays.

Figure 6 contains plots comparing the experimental time series with the predictions obtained from the tWhitham and sWhitham equations for the same experiment.

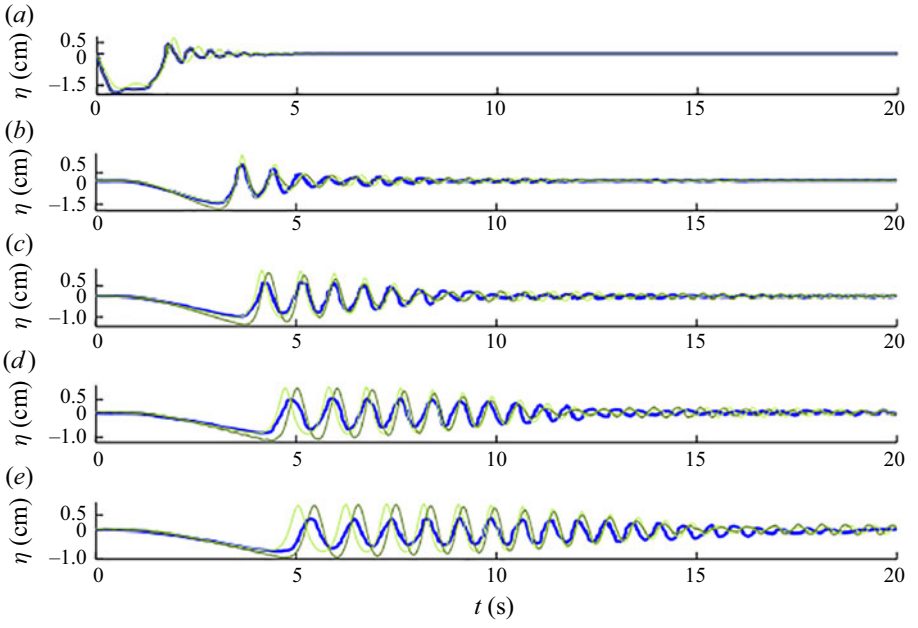

Figure 6. The experimental times series (blue curve) from the Hammack & Segur (1978) experiment using $A_0 = 1.5$ cm with the predictions obtained from the tWhitham (light green curve) and sWhitham (dark green curve) equations. The plots are ordered from (*a*) to (*e*) by increasing distance from the wavemaker.

The differences between the tWhitham and sWhitham predictions are smaller than the differences between the tKdV and sKdV predictions. Note that part of the error in the tWhitham prediction is due to the fact that the initial surface displacement is estimated. Again, this highlights a shortcoming of the temporal equations. Both the tWhitham and sWhitham equations overpredict the amplitudes of the waves at the downstream gauges due to their conservative nature, see § 3.3.

The predictions from all four models (tKdV, sKdV, tWhitham and sWhitham) for the Hammack & Segur (1978) experiment with $A_0 = 0.5$ cm (plots omitted for conciseness) are more accurate than those in the $A_0 = 1.5$ cm case. However, the results were qualitatively the same: the spatial equations provide more accurate predictions than do the temporal equations; the Whitham equations provide more accurate predictions than do the KdV equations; all four equations overpredicted the wave amplitudes. Finally, we note that linear theory is not sufficient to model the time series from either the $A_0 = 0.5$ cm or $A_0 = 1.5$ cm experiments. Predictions obtained from linear theory (plots omitted for conciseness) are significantly worse than any of the models examined herein.

Using the wave tank described above, Hammack & Segur (1974) conducted another series of experiments in which the piston was rapidly moved upwards at the start of the experiment. Time series were recorded at $x = 61$, 161, 961 and 2061 cm from the upstream end of the tank. The experimental data from the first gauge was used as the initial condition for the spatial equations. For the temporal equations, we used the following initial condition:

$$\eta(x,0) = \begin{cases} 0 & -7869 \leqslant x < -183, \\ 0.075 - 0.075\,\mathrm{sn}(0.0925434x, 0.9999^2) & -183 \leqslant x \leqslant 61, \\ 0 & 61 < x \leqslant 7747. \end{cases} \tag{3.2}$$

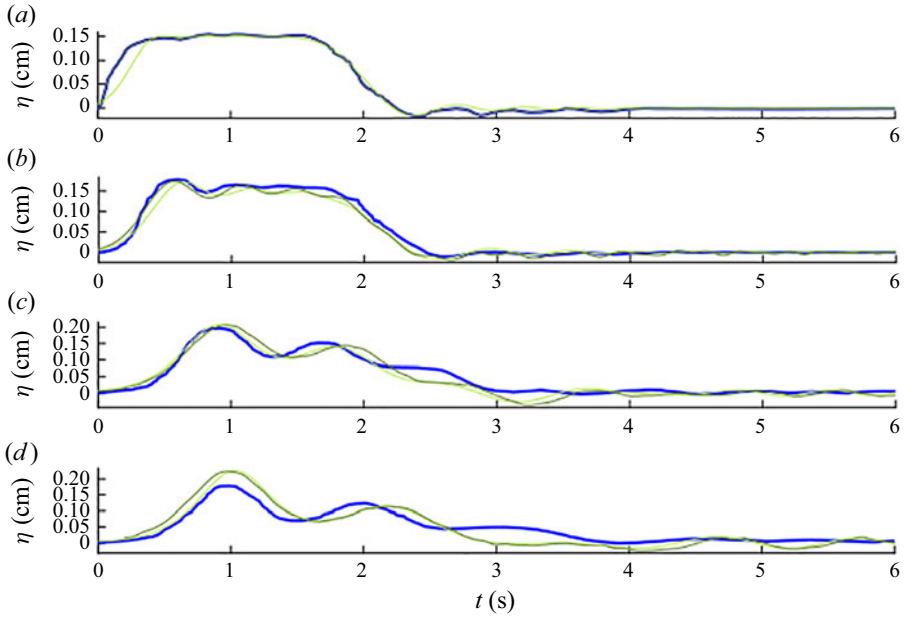

Figure 7. The experimental times series (blue curve) from one of the Hammack & Segur (1974) experiments with the predictions obtained from the tWhitham (light green curve) and sWhitham (dark green curve) equations. The plots are ordered from (*a*) to (*d*) by increasing distance from the wavemaker.

Figure 7 contains plots comparing the experimental times series with the predictions obtained from the tWhitham and sWhitham equations. The predictions from the tKdV and sKdV equations are similar. Both equations do reasonable jobs modelling the experimental data and the accuracy of the models is approximately the same as it is for the waves of depression experiments discussed above.

3.3. *Dissipative models of waves of depression on shallow water*

Figures 5 and 6 show that the tKdV, sKdV, tWhitham and sWhitham equations overpredict the amplitudes of the waves measured in the experiments. This overprediction is due to the fact that the equations are conservative, while the experiments contain dissipation. Figure 8 shows that the dimensional quantity

$$\mathcal{M}(x) = \frac{1}{\tau}\int_0^\tau \eta(x,t)^2\,\mathrm{d}t, \tag{3.3}$$

where τ is the dimensional length of the time series, decays nearly exponentially as the waves travel down the tank for both the $A_0 = 0.5$ cm and $A_0 = 1.5$ cm experiments. In order to address this, we consider the dimensional dissipative sKdV equation

$$\eta_x + \frac{1}{\sqrt{gh_0}}\,\eta_t - \frac{\sqrt{gh_0}}{6g^2}\,\eta_{ttt} - \frac{3}{2h_0\sqrt{gh_0}}\,\eta\eta_t + \delta\eta = 0, \tag{3.4}$$

and propose the following *ad hoc*, dimensional dissipative generalization of the sWhitham equation:

$$\eta_x + \sqrt{\frac{h_0}{g}}\,\mathcal{K}^{-1}(\omega) * \eta - \frac{3}{2h_0\sqrt{gh_0}}\,\eta\eta_t + \delta\eta = 0. \tag{3.5}$$

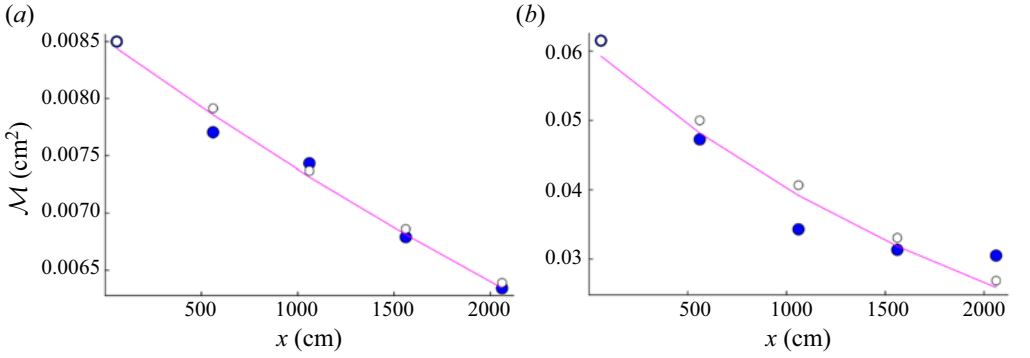

Figure 8. Plots of $\mathcal{M}$ versus x for the Hammack & Segur (1978) experiments with (*a*) $A_0 = 0.5$ cm and (*b*) $A_0 = 1.5$ cm. The blue dots represent the experimental measurements, the magenta curves represent the best-fit exponentials of the experimental data and the black circles represent the dsWhitham predictions.

Here δ is a non-negative constant representing the sum total of all forms of dissipation in the experiment. We refer to (3.4) and (3.5) as the dissipative sKdV (dsKdV) and the dissipative sWhitham (dsWhitham) equations, respectively. These equations predict that $\mathcal{M}$ will decay exponentially as x increases (i.e. as the waves travel down the tank). The single free parameter, δ, is determined by best fitting the measured exponential decay of $\mathcal{M}$. The δ values for the $A_0 = 0.5$ cm and $A_0 = 1.5$ cm experiments are 7.14×10^{-5} cm^{-1} and 2.07×10^{-4} cm^{-1}, respectively. This form of dissipation assumes that waves of all periods decay with the same rate. It is not a wavenumber-dependent form of dissipation.

Figure 9 shows comparisons between the experimental time series and predictions from the dsKdV and dsWhitham equations. The dsKdV equation does a reasonable job, but incorrectly models the phase speeds. The dsWhitham equation does an excellent job modelling the $A_0 = 1.5$ cm experimental time series. The predictions obtained from the dsWhitham equation are much better than those obtained from the conservative models. The results for the $A_0 = 0.5$ cm experiment (not shown) are similarly excellent.

3.4. *Solitons on shallow water*

We conducted experiments on solitons in a 1524 cm long (reflected waves did not impact the evolving soliton), 25.4 cm wide wave channel in the W.G. Pritchard Fluid Mechanics Laboratory. The tank is described in detail in Vasan *et al.* (2017). Briefly, the channel was cleaned with alcohol and filled with water to a desired depth. A wind was blown over the water surface along the length of the channel, creating a surface current that carried surface contaminants to the other end, where they were vacuumed with a wet-vac. The depth was then measured to be 5.30 cm. We generated solitons using a horizontal displacement of a piston: a vertical plate that spanned the width and height of the channel. The piston was programmed using the approach of Goring & Raichlen (1980), to take into account the real-time displacement of the plate. This approach and the details for our wavemaker are spelled out in Hammack *et al.* (2004). Herein, the wavemaker produced a repeatable soliton solution of the KdV equation with the desired height of 2.00 cm. Hammack *et al.* (2004) also generated a soliton solution of KdV with that height in water of depth 5.00 cm. They measured the spatial wavelength of the soliton to be approximately 80 cm. We did not measure a spatial wavelength, but the ratio in the present experiments is nearby this value. Therefore, the ratio of depth to wavelength, $r = h_0/\lambda \approx 0.066$, meaning these experiments are in the shallow-water regime. A capacitance-type wave gauge was used to measure the

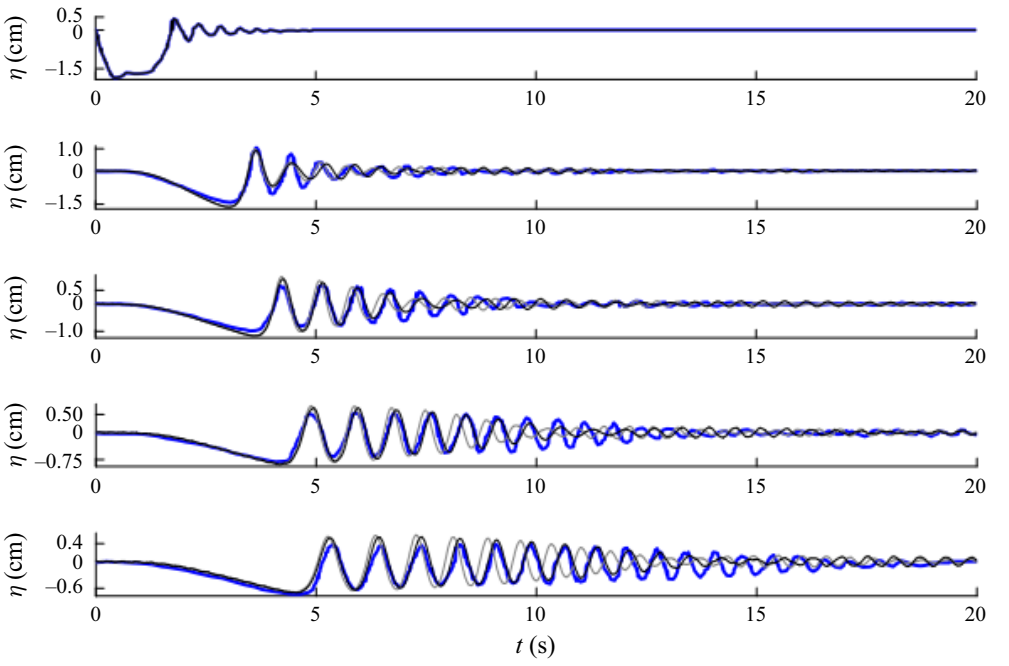

Figure 9. The experimental time series (blue curve) from the Hammack & Segur (1978) experiment using $A_0 = 1.5$ cm and the predictions obtained from the dsKdV (grey curve) and dsWhitham (black curve) equations.

surface displacement. For a fixed soliton amplitude, we conducted seven experiments with the wave gauge moved to the different x-locations, $x = 50, 150, 250, 350, 450, 550, 650$ cm away from the piston in its rest position. In these seven experiments, the start time of the paddle was not synced to the start time of data collection, so that the time series had to be shifted by hand to match comparisons; hence, we did not test accuracy of wave speed.

Figure 10 shows a comparison of the experimental time series and the predictions obtained from the dsWhitham equation for all seven gauges. The predictions line-up very closely with the experimental measurements. Figure 11 shows comparisons of the experimental time series and the predictions from the sKdV, dsKdV, sWhitham and dsWhitham equations for the last gauge. Although these experiments involve waves of elevation instead of waves of depression, the results are similar to those presented in the previous two subsections. The sWhitham predictions are more accurate than the sKdV predictions. The dsWhitham equation more accurately models the experimental time series than did the sWhitham equation. Other plots (omitted for conciseness) show that the dsWhitham equation is more accurate than the tKdV and sKdV equations. Additionally, the spatial equations more accurately predict the wave evolution than do the temporal equations.

3.5. *Waves of depression and elevation on deep water*

The tWhitham and sWhitham equations were proposed as models for waves on shallow water. However, they accurately reproduce the phase speeds of all unidirectional linear waves, regardless of the (uniform) depth of water. Because of this, it is reasonable to ask whether these equations accurately predict the evolution of waves on deep water.

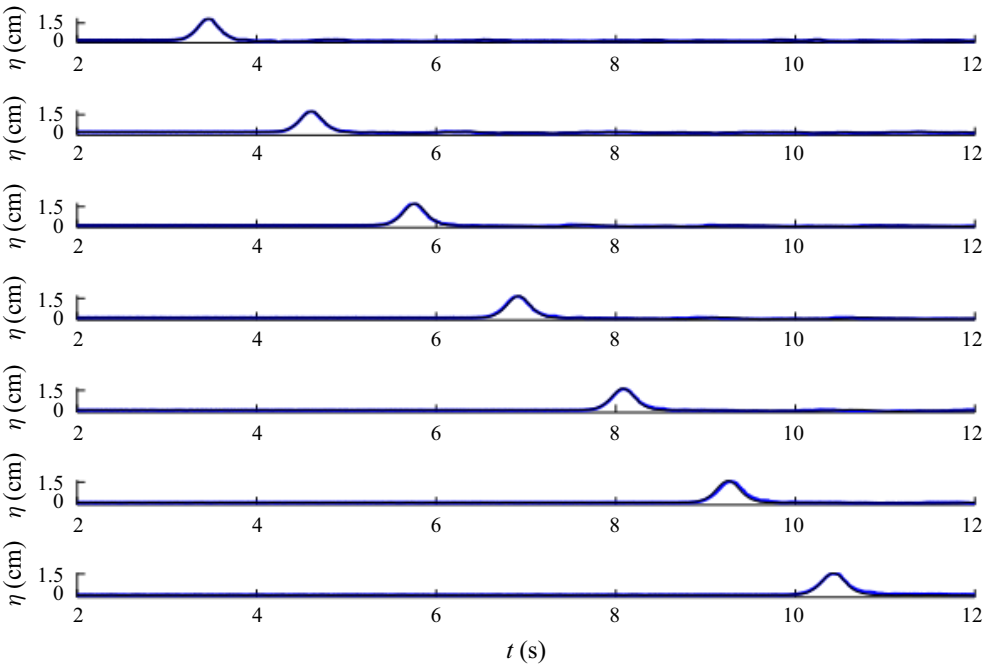

Figure 10. The experimental time series (blue curve) from the experiment described in § 3.4 along with the prediction obtained from the dsWhitham equation (black curve). The plots are ordered by increasing distance from the wavemaker.

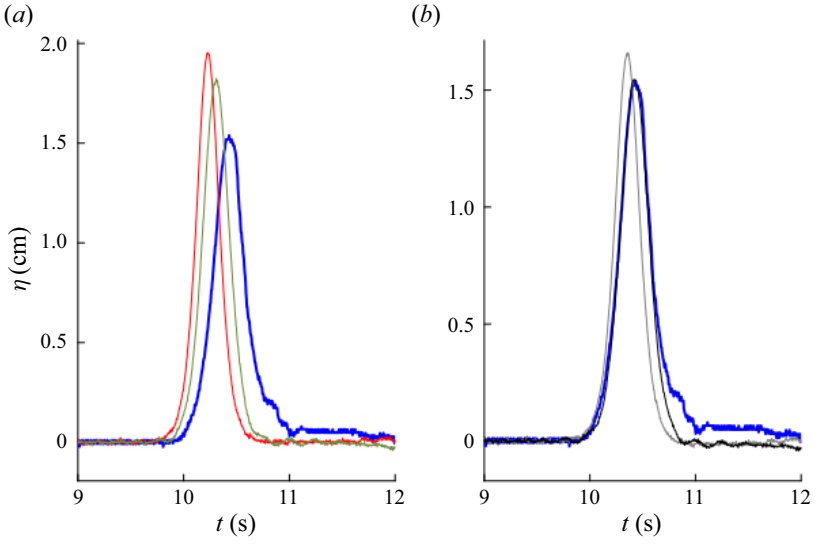

Figure 11. The experimental time series (blue curve) from the final gauge of the experiment described in § 3.4 along with the predictions obtained from (*a*) the sKdV (red curve) and sWhitham (dark green curve) equations and (*b*) the dsKdV (grey curve) and dsWhitham (black curve) equations.

In this section, we address this question by comparing predictions from the tWhitham and sWhitham equations with time series from our experiments of waves on deep water that are similar to those discussed above in §§ 3.2 and 3.3. In particular, we created an initial, localized, positive surface displacement and an initial, localized negative surface displacement. These surface displacements were created in the same tank used for the soliton experiments (see § 3.4) but with a horizontally aligned piston that had a vertical displacement. The piston for the experiments in this section was a horizontal plate that was 25.4 cm long in the x-direction, 1 cm tall in the vertical direction and spanned the width of the tank. The initial wave had a length of $\lambda = 50.8$ cm, and the depth was approximately $h_0 = 20$ cm. The resulting ratio of fluid depth to wavelength was $r = h_0/\lambda = 0.393$, with $\tanh(2\pi h_0/\lambda) = 0.986$, so that the waves were effectively in the deep-water regime.

The plate was impulsively lowered or raised 0.75 cm. To obtain the motion, the operator moved a Two-Servo Joystick, which sent a signal to a Servo Travel Tuner, in which we had programmed the desired plate displacement, and then to a Hi-Tec Linear Servo, which provided the plate motion. (All parts were from www.servocity.com.) There was a vertical barrier behind the plate so that the resulting waves were forced to travel in the $x > 0$ direction.

For the positive initial displacement, the tank was filled, and the surface was cleaned as described above to a depth of 20.18 cm. The plate was levelled parallel to the quiescent water surface and submerged 0.25 cm. It was dropped 0.75 cm impulsively, creating a localized positive surface displacement. Four *in situ*, capacitance wave gauges, located at $x = 4.0$, 225.5, 461.4, 679.0 cm from the edge of the plate, provided time series. Figure 12 shows the results. The data from the first gauge are used as the initial conditions for the spatial equations, so the model output and measurements agree exactly at that location. At the second gauge site, all three models predict well the oscillations that develop near the initial displacement and the wave packet that forms farther downstream. Dissipation becomes important in the surface displacement evolution by the third wave gauge. The conservative predictions agree qualitatively with the data, while the dsWhitham agrees both qualitatively and quantitatively, matching quite well even the radiation. By the fourth gauge, the agreement between the conservative predictions and the data worsens. The sWhitham prediction more accurately models the phase velocities than does the sKdV equation. The dsWhitham equation continues to produce a good quantitative comparison with the data.

For the negative initial displacement, the tank was filled, and the surface was cleaned as described above to a depth of 20.22 cm. The plate was levelled parallel to the quiescent water surface and submerged 0.75 cm. It was lifted 0.75 cm impulsively, creating a localized negative surface displacement. The four *in situ*, capacitance wave gauges, located at $x = 4.0$, 225.6, 462.5, 679.0 cm from the edge of the plate, provided time series. Figure 13 shows the results. The data from the first gauge is used as the initial condition, so the model output and measurements agree. Similar to the negative displacement experiments, all three models predict reasonably well the measured surface displacement at the second gauge site. Results from the sKdV and sWhitham equations are in qualitative agreement with data at the third and fourth gauge sites, while the dsWhitham equation predicts quite well the measured time series at the third and fourth gauge sites.

The sKdV predictions are less accurate than the sWhitham predictions due to phase velocity issues. Comparisons with sKdV and dsKdV are similar, although they do not align with the experimental data as well.

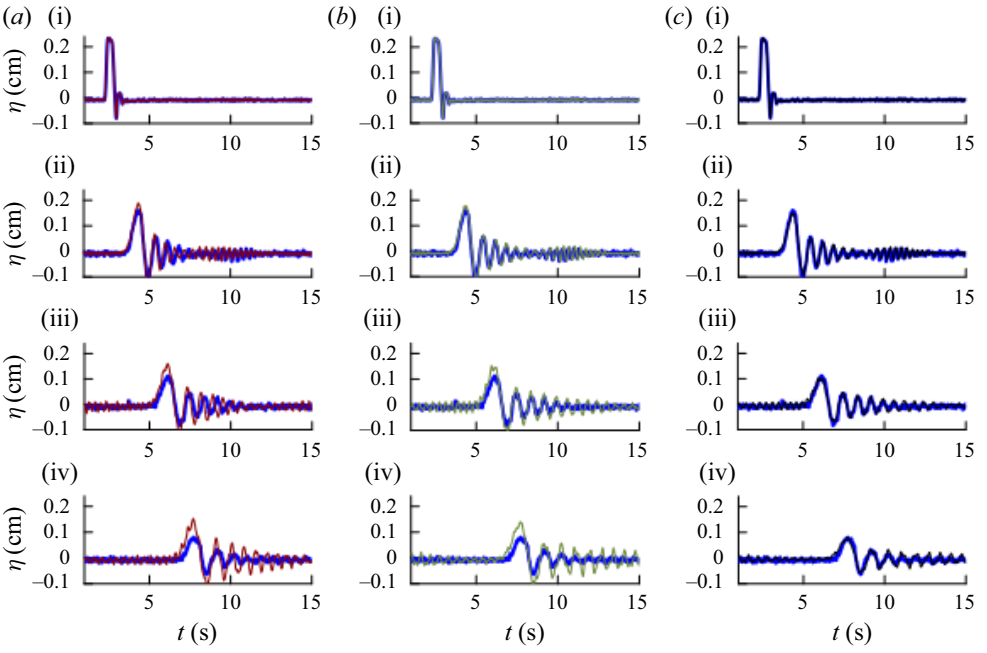

Figure 12. Comparisons of predictions from the (*a*) sKdV equation, (*b*) sWhitham equation and (*c*) dsWhitham equation when the initial surface displacement is positive. The blue curves correspond to the measured surface displacement, the red, dark green and black curves correspond to the sKdV, sWhitham and dsWhitham predictions, respectively. The plots are ordered from (i) to (iv) by increasing distance from the plate/wavemaker.

3.6. *Wave packets on deep water*

In order to further test the range of validity of the sWhitham and dsWhitham equations, we compare their predictions with experimental measurements of wave packets on deep water. Segur *et al.* (2005) showed that the dissipative nonlinear Schrödinger (dNLS) equation provided much more accurate predictions, both quantitatively and qualitatively, than did the nonlinear Schrödinger (NLS) equation for the experiments discussed in this section. They also showed that although plane-wave solutions to the NLS equation are unstable with respect to the modulational instability (also known as the sideband instability), uniform-amplitude solutions to the dNLS equation are stable with respect to the modulational instability. Finally, they showed that although the dNLS equation is stable with respect to the modulational instability, the sidebands may grow a limited amount.

In the Segur *et al.* (2005) experiments, the wave tank was 1311 cm long, 25.4 cm wide, had glass sidewalls and bottom and had a constant water depth of $h_0 = 20$ cm. A plunger-type wavemaker that spanned the width of the tank, had an exponential cross-section, and oscillated vertically was located at one end of the tank. The wavemaker created slowly modulated wavetrains with waves of wavelength $\lambda \approx 15$ cm. Since the ratio $r = h_0/\lambda \approx 1.33$ and $\tanh(2\pi h_0/\lambda) \approx 1.00$, this experiment is in the deep-water regime.

Figure 14 shows comparisons between the time series recorded in an experiment from § 6.2 of Segur *et al.* (2005) and the predictions from the sWhitham equation. Due to the complexity of the time series, we compare the magnitudes of the dominant Fourier coefficients instead of the time series themselves. The carrier wave frequency was $f_0 = 3.33$ Hz. The perturbation frequency was $f_p = 0.17$ Hz. So the sideband frequencies

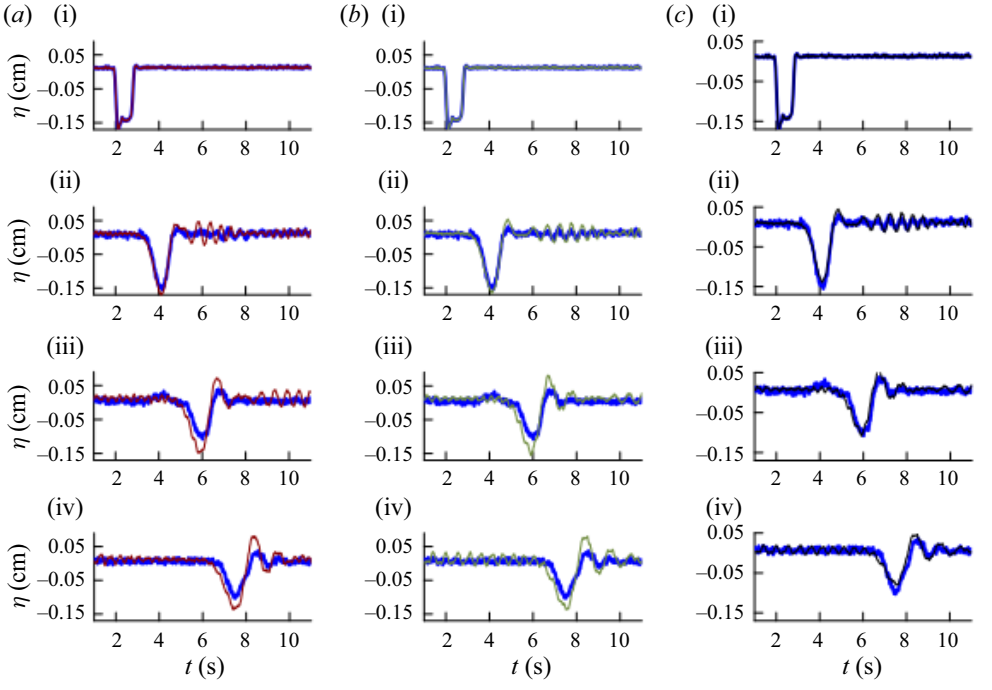

Figure 13. Comparisons of predictions from the (*a*) the sKdV equation, (*b*) sWhitham equation and (*c*) dsWhitham equation when the initial surface displacement is negative. The blue curves correspond to the measured surface displacement, the red, dark green and black curves correspond to the sKdV, sWhitham and dsWhitham predictions, respectively. The plots are ordered from (i) to (iv) by increasing distance from the plate/wavemaker.

were $f_{\pm n} = f_0 \pm nf_p$, for $n = 1, 2, 3$. Figure 14(*a*) shows the evolution of the carrier wave and figure 14(*b–g*) show the six most dominant sidebands. The plots show that the sWhitham equation does not accurately predict the evolution of these Fourier coefficients. This discrepancy appears to be related to the modulational instability. The experimental sidebands grow in magnitude as the waves travel down the tank (the experimental parameters were chosen so that the sidebands would grow), while the sWhitham equation predicts no such growth. This is consistent with the fact that the sWhitham equation is not unstable with respect to the modulational instability. An accurate model of this experimental data must allow for the sidebands to grow.

Figure 15 shows comparisons between the same experimental data and the predictions from the dsWhitham equation. These plots show that the dsWhitham equation does not accurately model the experimental data either. Though, note that the dsWhitham equation accurately models the evolution of the carrier wave. Similar results are obtained when the other three deep-water experiments from Carter, Henderson & Butterfield (2018) are examined. Therefore, it does not appear that the sWhitham or the dsWhitham equation can accurately model the evolution of wave packets on deep water.

4. Summary

We examined both the mathematical properties and applications of the sWhitham equation. Our main result is that the sWhitham equation performs better than the tWhitham

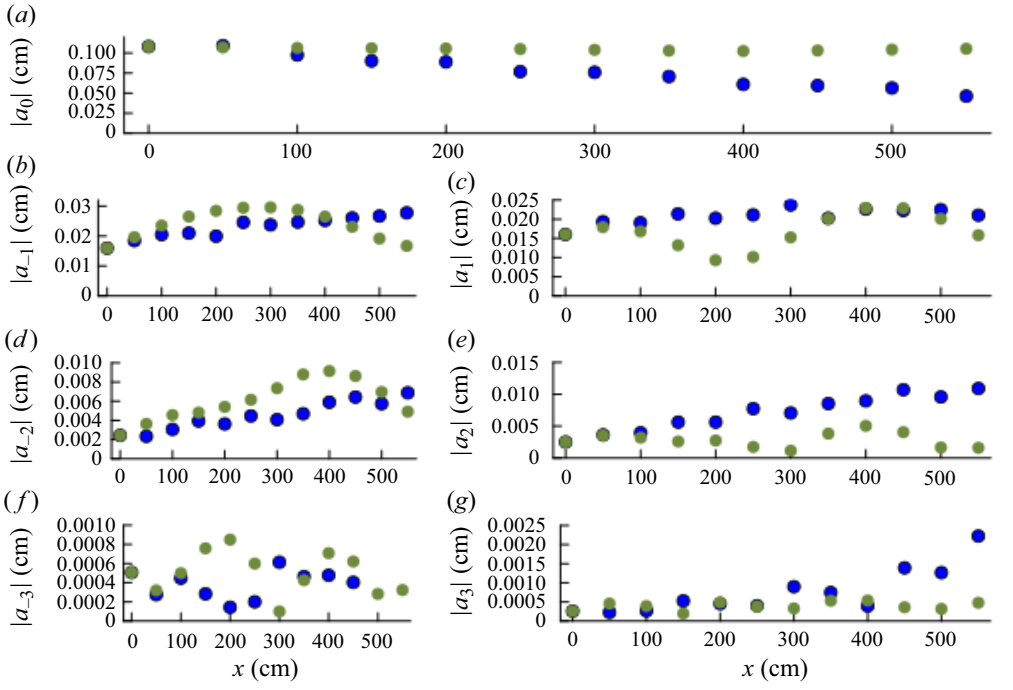

Figure 14. Plots comparing the experimental measurements (blue dots) from the deep-water experiment described in § 6.2 of Segur *et al.* (2005) with the predictions from the sWhitham equation (dark green dots). Panel (*a*) is the carrier wave and (*b–g*) are the six most dominant sidebands.

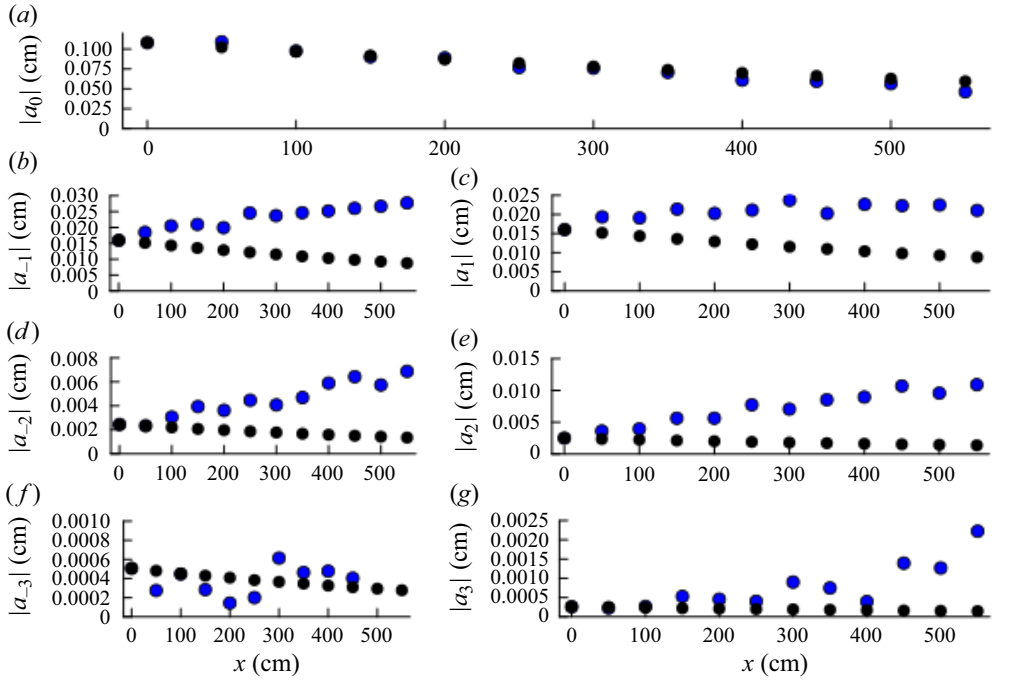

Figure 15. Plots comparing the experimental measurements (blue dots) from the deep-water experiment described in § 6.2 of Segur *et al.* (2005) with the predictions from the dsWhitham equation (black dots). Panel (*a*) is the carrier wave and (*b–g*) are the six most dominant sidebands.

equation and the spatial and temporal KdV equations for the experiments in both shallow and deep water considered here.

The sWhitham equation can be used to model how time series of surface displacement evolve as waves travel in space. Our analysis shows that the sWhitham equation admits periodic travelling-wave solutions, but does not appear to admit a periodic travelling-wave solution with maximal height. The sWhitham equation admits some solutions that are non-monotonic. Small- and moderate-amplitude travelling-wave solutions to the sWhitham equation are stable with respect to the modulational instability. Some larger-amplitude travelling-wave solutions are stable while others are unstable depending on wave period and wave height. There does not appear to be a simple relation between wave period and height that determines stability or instability.

Our comparisons with experiments show that for waves of depression and solitons on shallow water, the sWhitham equation provides more accurate predictions for experimental time series than do the tWhitham, tKdV and sKdV equations. Part of the reason that the spatial predictions are more accurate than the temporal predictions is that the initial conditions need to be approximated in the temporal case. Although the sWhitham equation was proposed as a model for shallow-water waves, we show that the sWhitham equation accurately models the evolution of initial waves of depression and elevation on deep water. The predictions obtained from the sWhitham equation are improved by adding dissipation. Finally, neither the sWhitham nor the dsWhitham equation accurately models the evolution of wave packets on deep water.

Acknowledgements. We thank R. Geist for constructing the laboratory apparatus, including the mechanical components, the motion control and the computer interfaces, for the shallow-water soliton and all of the deep-water experiments. We thank V. Vasan for writing the wavemaker program for experiments on the shallow-water soliton and the deep-water wave packets. We thank R. Crable for building and maintaining the capacitance wave gauges. We thank K. Hammack for digitizing the experimental data from Hammack & Segur (1978). We thank E. Byrnes for helpful discussions.

Funding. J.D.C. and P.P. thank the Dirección General de Asuntos del Personal Académico (DGAPA) at the Universidad Nacional Autónoma de México (UNAM) for a Programa de Estancias de Investigación (PREI) grant that supported J.D.C.'s sabbatical stay at UNAM. P.P. acknowledges partial support by PAPIIT IG100522.

Declaration of interests. The authors report no conflict of interest.

Author ORCID.
John D. Carter https://orcid.org/0000-0003-3380-5924.

Appendix A. Conserved quantities

The conserved quantities for the non-dimensional temporal KdV equation are

$$\mathcal{Q}_1 = \int_0^L u \, \mathrm{d}\chi, \tag{A1a}$$

$$\mathcal{Q}_2 = \int_0^L u^2 \, \mathrm{d}\chi, \tag{A1b}$$

$$\mathcal{Q}_3 = \tfrac{1}{2} \int_0^L \left(u^2 + \tfrac{1}{6} u_\chi^2 - \tfrac{1}{2} u^3 \right) \mathrm{d}\chi, \tag{A1c}$$

where L is the χ-period of the solution. The conserved quantities for the non-dimensional tWhitham equation are $\mathcal{Q}_1$, $\mathcal{Q}_2$ and

$$\mathcal{Q}_4 = \frac{1}{2}\int_0^L \left(u\left(\frac{K(k)}{i\,k}\right) * u - \frac{1}{2}u^3 \right) \mathrm{d}\chi. \tag{A2}$$

These quantities are conserved in τ.

The conserved quantities for the non-dimensional sKdV equation are

$$\mathcal{Q}_5 = \int_0^T u\,\mathrm{d}\tau, \tag{A3a}$$

$$\mathcal{Q}_6 = \int_0^T u^2\,\mathrm{d}\tau, \tag{A3b}$$

$$\mathcal{Q}_7 = \tfrac{1}{2}\int_0^T \left(u^2 + \tfrac{1}{6}u_\tau^2 - \tfrac{1}{2}u^3 \right) \mathrm{d}\tau, \tag{A3c}$$

where T is the τ-period of the solution. The conserved quantities for the non-dimensional sWhitham equation are $\mathcal{Q}_5$, $\mathcal{Q}_6$ and

$$\mathcal{Q}_8 = \frac{1}{2}\int_0^T \left(u\left(\frac{K^{-1}(w)}{i\,w}\right) * u - \frac{1}{2}u^3 \right) \mathrm{d}\tau. \tag{A4}$$

These quantities are conserved in χ.

References

Ablowitz, M.J. & Segur, H. 1981 *Solitons and the Inverse Scattering Transform*. SIAM.

Agrawal, G. 2019 *Nonlinear Optics*, 6th edn. Academic.

Ali, A. & Kalisch, H. 2014 On the formulation of mass, momentum and energy conservation in the KdV equation. *Acta Appl. Math.* **133**, 113–131.

Benjamin, T.B. & Feir, J.E. 1967 The disintegration of wave trains on deep water: part I. Theory. *J. Fluid Mech.* **27**, 417–430.

Binswanger, A.L., Hoefer, M.A., Ilan, B. & Sprenger, P. 2021 Whitham modulation theory for generalized Whitham equations and a general criterion for modulational instability. *Stud. Appl. Maths* **147**, 724–751.

Bottman, N. & Deconinck, B. 2009 KdV cnoidal waves are linearly stable. *Discrete Continuous Dyn. Syst.* A **25**, 1163–1180.

Bruell, G. & Pei, L. 2023 Symmetry of periodic traveling waves for nonlocal dispersive equations. *SIAM J. Math. Anal.* **55**, 486–507.

Byrd, P.F. & Friedman, M.D. 1971 *Handbook of Elliptic Integrals for Scientists and Engineers*. Springer.

Carter, J.D. 2018 Bidirectional Whitham equations as models of waves on shallow water. *Wave Motion* **82**, 51–61.

Carter, J.D. 2024 Instability of near-extreme solutions to the Whitham equation. *Stud. Appl. Maths.* **152** (3), 903–915.

Carter, J.D., Francius, M., Kharif, C., Kalisch, H. & Abid, M. 2023 The superharmonic instability and wave breaking in Whitham equations. *Phys. Fluids* **35**, 103609.

Carter, J.D., Henderson, D.M. & Butterfield, I. 2018 A comparison of frequency downshift models of wave trains on deep water. *Phys. Fluids* **31**, 013103.

Carter, J.D., Kalisch, H., Kharif, C. & Abid, M. 2022 The cubic-vortical Whitham equation. *Wave Motion* **110**, 102883.

Deconinck, B. & Kutz, J.N. 2006 Computing spectra of linear operators using Hill's method. *J. Comput. Phys.* **219**, 296–321.

Deconinck, B. & Nivala, M. 2010 Periodic finite-genus solutions of the KdV equation are orbitally stable. *Physica* D **239**, 1147–1158.

DECONINCK, B. & OLIVERAS, K. 2011 The instability of periodic surface gravity waves. *J. Fluid Mech.* **675**, 141–167.

DECONINCK, B. & TRICHTCHENKO, O. 2015 High-frequency instabilities of small-amplitude Hamiltonian PDEs. *Discrete Continuous Dyn. Syst.* **37** (3), 1323–1358.

EHRNSTRÖM, M. & KALISCH, H. 2009 Traveling waves for the Whitham equation. *Diff. Integral Equ.* **22**, 1193–1210.

EHRNSTRÖM, M. & WAHLÉN, E. 2019 On Whitham's conjecture of a highest cusped wave for a nonlocal dispersive equation. *Ann. Inst. Henri Poincaré* **36**, 769–799.

GORING, D.G. & RAICHLEN, F. 1980 The generation of long waves in the laboratory. In *Coastal Engineering Proceedings, Sydney, Australia*, vol. 1, p. 46.

HAMMACK, J. 1973 A note on tsunamis: their generation and propagation in an ocean of uniform depth. *J. Fluid Mech.* **60**, 769–799.

HAMMACK, J., HENDERSON, D., GUYENNE, P. & YI, M. 2004 Solitary-wave collisions. In *Proceedings of the 23rd ASME Offshore Mechanics and Arctic Engineering. A Symposium to Honor Theodore Yao-Tsu Wu*. World Scientific.

HAMMACK, J.L. & SEGUR, H. 1974 The Korteweg-de Vries equation and water waves. Part 2. Comparison with experiments. *J. Fluid Mech.* **65**, 289–314.

HAMMACK, J.L. & SEGUR, H. 1978 The Korteweg-de Vries equation and water waves. Part 3. Oscillatory waves. *J. Fluid Mech.* **84**, 337–358.

HUR, V.M. & JOHNSON, M.A. 2015 Modulational instability in the Whitham equation for water waves. *Stud. Appl. Maths* **134** (1), 120–143.

JOHNSON, R.S. 2001 *A Modern Introduction to the Mathematical Theory of Water Waves*. Cambridge University Press.

KORTEWEG, D.J. & DE VRIES, D. 1895 On the change of form of long waves advancing in a rectangular canal, and on a new type of long stationary wave. *Phil. Mag.* **39**, 422–443.

LANNES, D. 2013 *The Water Waves Problem: Mathematical Analysis and Asymptotics*. American Mathematical Society.

MANAKOV, S.V. 1974 On the theory of two-dimensional stationary self-focusing of electromagnetic waves. *Sov. Phys. JETP* **38**, 248–253.

MILES, J.W. 1981 The Korteweg-de Vries equation, a historical essay. *J. Fluid Mech.* **106**, 131–147.

RUSSELL, J.S. 1844 Report on waves. In *Report of the Fourteenth Meeting of the British Association for the Advancement of Science, York*, pp. 311–390.

SANFORD, N., KODAMA, K., CARTER, J.D. & KALISCH, H. 2014 Stability of traveling wave solutions to the Whitham equation. *Phys. Lett.* A **378**, 2100–2107.

SEGUR, H., HENDERSON, D., CARTER, J.D., HAMMACK, J., LI, C., PHEIFF, D. & SOCHA, K. 2005 Stabilizing the Benjamin–Feir instability. *J. Fluid Mech.* **539**, 229–271.

TRILLO, S., KLEIN, M., CLAUSS, G.F. & ONORATO, M. 2016 Observation of dispersive shock waves developing from initial depressions in shallow water. *Physica* D **333**, 276–284.

VASAN, V.V., OLIVERAS, K., HENDERSON, D. & DECONINCK, B. 2017 A method to recover water-wave profiles from pressure measurements. *Wave Motion* **75**, 25–35.

WHITHAM, G.B. 1967 Variational methods and applications to water waves. *Proc. R. Soc. Lond.* A **299**, 6–25.

WHITHAM, G.B. 1974 *Linear and Nonlinear Waves*. Wiley.

YOSHIDA, H. 1990 Construction of higher order symplectic integrators. *Phys. Lett.* A **150**, 262–268.

ZABUSKY, N.J. & GALVIN, C.J. 1971 Shallow-water waves, the Korteweg-de Vries equation and solitons. *J. Fluid Mech.* **47**, 811–824.